



# A splicing variant in *EFCAB7* hinders ciliary transport and disrupts cardiac development

Received for publication, December 16, 2024 Published, Papers in Press, January 31, 2025,  
<https://doi.org/10.1016/j.jbc.2025.108249>

Xin Yang<sup>1,2,3,†</sup>, Qiuye Wang<sup>1,2,†</sup>, Tianyuan Li<sup>3,†</sup>, Yan Zhou<sup>1,2</sup>, Jimiao Gao<sup>1,2</sup>, Wanting Ma<sup>1,2</sup>, Na Zhao<sup>1,2</sup>,  
 Xinyue Liu<sup>1,2</sup>, Zihe Ai<sup>3</sup>, Steven Y. Cheng<sup>3</sup>, Yayun Gu<sup>1,2</sup>, Bijun Zhao<sup>4,\*</sup>, Shen Yue<sup>3,\*</sup>, and Zhibin Hu<sup>1,2,\*</sup> 

From the <sup>1</sup>State Key Laboratory of Reproductive Medicine, Nanjing Medical University, Nanjing, Jiangsu, China; <sup>2</sup>School of Public Health, Center for Global Health, Nanjing Medical University, Nanjing, Jiangsu, China; <sup>3</sup>Department of Medical Genetics, Jiangsu Key Laboratory of Xenotransplantation, Nanjing Medical University, Nanjing, China; <sup>4</sup>Department of Cardiovascular Surgery, Xijing Hospital, The Fourth Military Medical University, Xi'an, China

Reviewed by members of the JBC Editorial Board. Edited by Paul Shapiro

The Tetralogy of Fallot (TOF), the most prevalent form of cyanotic congenital heart disease, stems from abnormal development of the outflow tract during embryogenesis. Despite the crucial role played by primary cilia in heart development, there is currently insufficient evidence to establish a causal relationship between defects in genes related to primary cilia and non-syndromic TOF. Here, we performed Sanger sequencing on 131 Chinese patients diagnosed with TOF and identified a splicing variant (c.683-1G > C) in the *EFCAB7* gene. This splicing variant triggered exon skipping, leading to the production of a non-functional protein both *in vitro* and *in vivo*. Mice carrying this variant exhibited abnormal cardiac development, impaired ciliogenesis, disrupted Hedgehog signaling, and hindered Shh/Gli pathway activity. Through the integration of CUT&Tag data on Glis and bulk RNA-seq profiles of embryonic hearts at E10.5, we found that transcriptional downregulation of Gli target genes, including *Myh6*, *Zfpml1*, and *Nkx2-5*, is a consequence of Shh signaling inhibition. Our findings implicate *EFCAB7* as a potential causative gene for TOF, underscoring the indispensable function of primary cilia in the intricate process of cardiac septation during heart development.

Congenital heart defects (CHD) arise from the structural or functional abnormalities of the heart and/or great vessels during embryogenesis (1). Around 1% of newborns suffer from CHD, which constitutes the primary cause of infant mortality worldwide (2, 3). CHD affects most parts of the heart and is classified into three main categories: cyanotic heart disease, left-sided obstructive defects, and septal defects (4). Among these, Tetralogy of Fallot (TOF) is the most common cyanotic CHD, including overriding aorta, pulmonary artery stenosis, ventricular septal defects, and right ventricular hypertrophy, accounting for nearly 10% of all cases (5). The etiology of CHD is multifactorial, including genetic and environmental factors. Currently, the major identified genetic causes involve

chromosomal abnormalities, large subchromosomal deletions or duplications as well as point mutations (6). As with other types of CHDs, TOF displays a significant degree of genetic heterogeneity (7, 8). Approximately 20% of TOF cases are classified as syndromic and are associated with recognized diseases or chromosomal abnormalities, such as 22q11 deletion syndrome (Di George syndrome) and Down's syndrome (9, 10). The remaining 80% of TOF cases are non-syndromic, with an unknown etiology (11, 12).

Over the past 2 decades, findings from genetic studies conducted on mice and large-scale sequencing of CHD patients have indicated that primary cilia play a crucial role in cardiovascular development (13–15). Primary cilia are membrane-bound organelles, based on microtubules, protruding from the surface of most animal cells during growth arrest. The axoneme of primary cilia comprises nine doublet microtubules extending from a basal body derived from the mother centriole of the centrosome (16). Due to the absence of the central apparatus and dynein arms, most primary cilia exhibit a “9 + 0” microtubule configuration. Consequently, primary cilia are usually non-motile, and serve a function akin to an “antenna” with numerous signaling receptors on them, and coordinate the transduction of multiple developmental signaling pathways, such as the Hedgehog (Hh) pathway (17, 18). Primary cilia are indispensable for Hh signaling output, and all core components of the Hh signaling machinery—ranging from the receptor PTCH1 and SMO to the GLI transcriptional effectors—dynamically localize to cilia during signal transduction (19, 20). A range of ciliary proteins collaborate to ensure normal ciliary transport, including components of the basal body that nucleates the cilium; the transition fibers that anchor the basal body to the cell surface; the transition zone that gates protein entry into the cilium; the motors that mediate intraciliary transport; and the intraflagellar transport (IFT) complexes that traffic ciliary cargo (19).

Impairment of the structures or functions of primary cilia results in abnormal signaling transduction, subsequently causing a series of syndromes collectively termed “ciliopathies” (21). Congenital cardiovascular deformities are observed in patients with certain ciliopathies, such as Bardet-Biedl

<sup>†</sup> These authors contributed equally to this work.

\* For correspondence: Zhibin Hu, [zhibin\\_hu@njmu.edu.cn](mailto:zhibin_hu@njmu.edu.cn); Shen Yue, [yueshen@njmu.edu.cn](mailto:yueshen@njmu.edu.cn); Bijun Zhao, [bijunzh@hotmail.com](mailto:bijunzh@hotmail.com).

## EFCAB7 splicing variant disrupts cilia function in heart development

syndrome, Joubert syndrome, Sensenbrenner syndrome, and Ellis van Creveld (EvC) syndrome (22). However, there is currently no evidence to suggest that non-syndromic TOF is associated with defects in the primary cilia genes.

Previous studies have identified EF-hand calcium binding domain 7 (EFCAB7) functions as a component of the EvC complex, located immediately distal to the ciliary transition zone, and functions as a positive regulator of the Hedgehog pathway. Depletion of *EFCAB7* leads to the mislocalization of EVC-EVC2 within cilia and inhibits the induction of Gli1 and Gli2, which are transcription factors in the Hh pathway (23, 24). In this study, we performed Sanger sequencing on 131 Chinese patients with non-syndromic TOF, constructed a mouse model of *EFCAB7* mutation based on the splice site variant found in *EFCAB7*, and conducted a mechanism study. Our data suggest that *EFCAB7* mutations are a disease factor in TOF, which affects the cardiac development process by hindering Sonic Hedgehog (Shh) signaling transduction in cilia.

### Results

#### A splice site variant of EFCAB7 identified in patients with TOF

First, we conducted Sanger sequencing of the exon regions of the *EFCAB7* gene in 131 patients with TOF and identified five mutations, including a splice acceptor mutation, that potentially affect the function of *EFCAB7* (Table S2). Subsequently, in a separate cohort of 682 patients with CHDs, we further validated the three mutations in the exons of this gene (Table S3). Among these eight mutations, our attention was drawn to a canonical splice site variation (c.683-1G > C) located at the last base of the adjacent intron preceding exon 6 of *EFCAB7*, potentially causing misrecognition of the splice donor site and inducing mRNA splicing errors, leading to loss of protein function (Fig. 1A). To validate this prediction, we conducted a minigene assay using the Exontrap Cloning Vector, pET01, which possesses an intrinsic splicing function that allows for the selective cloning of exon sequences from genomic eukaryotic DNA fragments. The 293T cells were transfected with pET01 carrying either wild-type (WT) or c.683-1G > C mutant *EFCAB7* minigenes, and the total RNA was reverse transcribed into cDNA for amplification and sequencing. Cells transfected with the WT minigene produced a 380 bp band upon PCR analysis. Direct sequencing of the PCR products revealed that it contained both Exon 5 and 6. In contrast, cells transfected with mutant minigene produced a shorter 258 bp band that skipped Exon 6 of *EFCAB7* (Fig. 1B). The observed results were consistent with the disruption of the genuine acceptor site of exon 6 due to the c.683-1G > C alteration. Subsequently, we aimed to further investigate the functionality of the abnormal *EFCAB7* transcript caused by the splice site variant. It is anticipated that the transcript lacking 122 bp of exon 6 would induce a reading frameshift, leading to premature termination of translation and ultimately production of non-functional protein products (Fig. 1C). To assess *EFCAB7* mRNA expression in mouse hearts, we designed forward and reverse primers targeting Exons 5 and 8 of the *EFCAB7* gene, as the mutation causes exon skipping and the

loss of Exon 7. The expression levels of *EFCAB7* mRNA were then quantified using RT-qPCR. Our results revealed that the expression of *EFCAB7* mRNA was significantly reduced in both the heterozygous and homozygous mutant mice hearts compared to the WT mice (Fig. 1D).

#### The splicing variant reduced EFCAB7 protein stability

To further assess the *EFCAB7* variant, we generated eukaryotic expression plasmids containing the complete sequence of *EFCAB7* cDNA and a mutant lacking 122 bp of exon 6 (referred to as EFCAB7mut) fused with EGFP. The Western blot analysis revealed that EFCAB7mut expressed truncated protein products of shorter length, but the mutation does not completely abolish EFCAB7 protein expression (Fig. 1E). Previous studies have identified EFCAB7 as a constituent of the EvC complex in primary cilia. In this study, we utilized immortalized human retinal pigment epithelial cell line RPE1 to investigate the subcellular localization of endogenous EFCAB7 protein and observed its presence at the basal body region of primary cilia (Fig. 1F). After transient transfection into RPE1 cells, we observed that EGFP-EFCAB7mut localized at the basal body of primary cilia similarly to EGFP-EFCAB7 (Fig. 1G). There was no significant alteration in the ciliary localization of the mutant protein.

We noticed that the fluorescence intensity of EGFP-EFCAB7mut was relatively weak, possibly due to decreased protein stability. To validate this hypothesis, we treated RPE1 cells expressing exogenous *EFCAB7* or its mutant with MG132 to inhibit proteasome-mediated degradation and observed a substantial accumulation of labeled protein (Fig. 1H). This finding suggests rapid turnover of EFCAB7 in RPE1 cells. Subsequently, we assessed the decay rate of EFCAB7 by blocking protein synthesis using cycloheximide (CHX). The half-life of EFCAB7mut protein was significantly shorter compared to WT (Fig. 1I), indicating reduced protein stability likely caused by abnormal folding of the truncated variant.

#### Aberrant cardiac development in Efcab7 mutant mice

While the missense variant of *EFCAB7* was previously reported to modify the phenotype of EvC syndrome (25, 26), a ciliopathy with cardiac anomalies, there is currently no direct evidence that it is responsible for abnormal cardiac development. We successfully generated knock-in mice using CRISPR/Cas9 technology and an ssDNA template carrying the patient-specific point variant (Fig. 2A). To mitigate off-target risks, we validated the top 10 predicted high-risk sites and found no off-target effects (Fig. S1). We extracted total RNA from the hearts of WT and *Efcab7*<sup>mut/mut</sup> mice, and performed reverse transcription and PCR amplification. Agarose gel electrophoresis and sequencing results confirmed the deletion of exon 6 in mutant mice (Fig. 2B). Upon conducting heterozygous intercrosses, we observed that *Efcab7*<sup>mut/mut</sup> mice were born at expected Mendelian ratios (Fig. 2C).

After staining the hearts of postnatal day 1 (P1) newborns, we observed normal heart development in WT mice. In contrast, we found overriding aorta in 2 of 51 (3.92%)

# EFCAB7 splicing variant disrupts cilia function in heart development

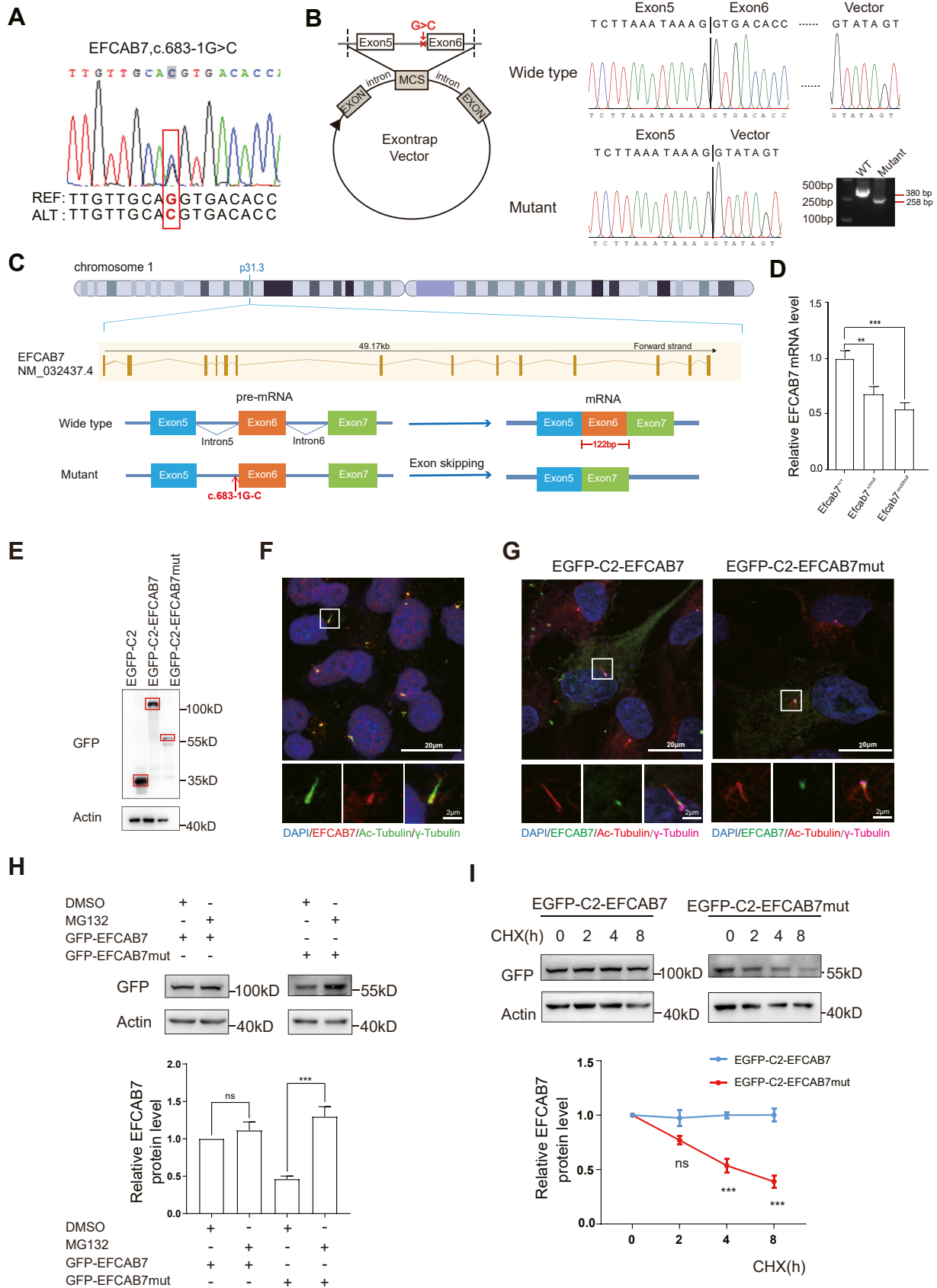


**Figure 1. An intronic variation of EFCAB7 leads to abnormal mRNA splice and reduced protein stability.** A, verification of an intronic variation in the EFCAB7 gene of a TOF patient by Sanger sequencing. B, cloning of the EFCAB7 minigene, comprising exons 5 to 6 and their flanking introns, into the Exontrap vector for *in vitro* splicing analysis. Agarose gel electrophoresis of amplified cDNA fragments from 293T cells expressing the ExonTrap minigene, revealing differences between wild-type (WT) and mutant constructs. Sanger sequencing confirms the RT-PCR products. C, schematic representation of the



## EFCAB7 splicing variant disrupts cilia function in heart development

*Efcab7*<sup>mut/mut</sup> mice, ventricular septal defects (VSD) in 3 of 51 (5.88%), and atrial septal defect (ASD) in 11 of 51 (21.57%). Additionally, we also found a certain number of heart defects in *Efcab7*<sup>+/mut</sup> mice (Fig. 2, D and E). Furthermore, the widths of the pulmonary artery in *Efcab7*<sup>mut/mut</sup> mice and *Efcab7*<sup>+/mut</sup> mice were both significantly narrower than those in WT mice (Fig. 2F). These findings indicate abnormal development of the cardiac outflow tract in *Efcab7*<sup>mut/mut</sup> mice.

### Aberrant ciliary transport of *Smo* in *Efcab7*<sup>mut/mut</sup> cells

Defects in the structure and function of primary cilia play a crucial role in the pathogenesis of CHD. Several kinds of ciliary mutant mice reveal CHD phenotype. Since *EFCAB7* functions in the EvC zone of primary cilia, we aimed to investigate whether the malformation of the cardiac outflow tract observed in *Efcab7*<sup>mut/mut</sup> mice was due to abnormal ciliogenesis. To achieve this, we immunostained the primary cilia of E13.5 embryonic hearts and found that the percentage of primary cilia in *Efcab7*<sup>mut/mut</sup> embryonic hearts was not significantly decreased, but their cilia length was shortened (Fig. 3A). To understand the functional changes of *Efcab7* mutant at the ciliary base, we isolated primary mouse embryo fibroblasts (MEFs) from E13.5 *Efcab7*<sup>mut/mut</sup> embryos and cultured them *in vitro*. After inducing ciliogenesis by low-serum stimulation of cultured cells for 24 h, we found a reduced proportion of ciliogenesis and shortened primary cilia of *Efcab7*<sup>mut/mut</sup> MEFs (Fig. 3B). These results indicated that the *Efcab7* mutant led to the abnormality of primary cilia.

In the Hh pathway, the dynamic localization of all core components, including the receptor PTCH1 and SMO, as well as the GLI transcriptional effectors, to primary cilia is essential for the signaling output. Therefore, we further explored the effect of the *Efcab7* variant on Hh signaling transduction. We used Sonic Hedgehog (Shh) ligands to stimulate *in vitro* cultured MEFs. After hours of Shh ligand stimulation, we observed the continuous accumulation of endogenous SMO in the primary cilia in *Efcab7*<sup>+/+</sup> MEFs by immunofluorescence staining, which reached saturation within 4 h (Figs. 3C, S2). However, in *Efcab7*<sup>mut/mut</sup> MEFs, SMO exhibited a delayed response to Shh ligand stimulation in terms of its enrichment in primary cilia. Specifically, SMO exhibited reduced accumulation in primary cilia after 1 to 2 h of Shh treatment, but eventually reached saturation within 4 h (Figs. 3C, S2). To conduct a deeper examination of the ciliary trafficking irregularities observed in *Efcab7*<sup>mut/mut</sup> MEFs, we utilized lentivirus to infect primary MEFs to stably express mCherry-tagged SMO. We next conducted a Fluorescence Recovery After

Photobleaching (FRAP) assay and found that the fluorescence recovery of SMO-mCherry in *Efcab7*<sup>mut/mut</sup> cilia was less than that in control cilia after photobleaching (Fig. 3D), suggesting a defected ciliary import of SMO in *Efcab7*<sup>mut/mut</sup> cilia. We also monitored the dynamics of SMO-mCherry through kymograph analysis. Neither the anterograde nor the retrograde velocities of SMO puncta were affected by *Efcab7* mutants (Fig. 3E). Meanwhile, the retrograde frequency of SMO puncta appeared to be slightly augmented in the cilia of *Efcab7*<sup>mut/mut</sup> MEFs, but its anterograde frequency remained unchanged, compared to the WT MEFs (Fig. 3E). These data indicated that the deficiency of *Efcab7* hinders the transportation of SMO in primary cilia.

### Shh/Gli pathway was impeded in *Efcab7*<sup>mut/mut</sup> cells and embryonic hearts

After stimulation with the Shh ligand, except for the ciliary aggregation of SMO, the downstream transcription factor GLI2 also accumulates at the tips of the primary cilia (Fig. 4A). However, Shh-induced GLI2 aggregation at the ciliary tips was significantly inhibited in *Efcab7*<sup>mut/mut</sup> MEFs (Fig. 4, A and B). *Gli1* was an early target gene induced by Shh signaling, and the levels of its protein and RNA products were significantly decreased in mutant cells (Fig. 4, C and D). Hh signaling also plays an essential role in cardiovascular development, including the development of the outflow tract and semilunar valve (27, 28). We suspected that the aberrant cardiac development observed in *Efcab7* mutant mice might be due to the inappropriate changes in Shh signaling, and we tested the activity of the Shh pathway in embryonic hearts. The Western blot results indicated that the expression of GLI1 was significantly reduced in E10.5 *Efcab7*<sup>mut/mut</sup> hearts compared to WT hearts (Fig. 4E) and suggested that the Shh/Gli pathway was impeded during the heart development of *Efcab7*<sup>mut/mut</sup> embryos.

We further conducted bulk RNA sequencing on E10.5 hearts from WT and *Efcab7*<sup>mut/mut</sup> mice, followed by an analysis to identify the intersection between 1786 significantly down-regulated genes in E10.5 *Efcab7*<sup>mut/mut</sup> hearts and 3949 target genes of Gli1/Gli2 identified from CUT&Tag results of E10.5 hearts of WT mice. This analysis resulted in a total of 431 GLI-binding genes that were down-regulated in the *Efcab7*<sup>mut/mut</sup> hearts (Fig. 4F). Among the top enriched pathways in GO enrichment analysis of these 431 genes, a quarter were associated with heart morphogenesis and development (Fig. 4G). Furthermore, we found that out of these 431 genes, seven have been previously reported to be associated with TOF (Table S4), and qPCR analysis revealed lower levels of RNA

splicing patterns observed for WT and mutant *EFCAB7* mRNA. D, the relative mRNA expression of *EFCAB7* in E10.5 WT, *Efcab7*<sup>+/mut</sup>, *Efcab7*<sup>mut/mut</sup> hearts. \*\**p* < 0.01, \*\*\**p* < 0.001. E, the protein levels assessed by Western blot for *EFCAB7* in RPE1 cells carrying wild-type or mutant cDNA. EGFP-C2 serves as the empty vector control. F, ciliary localization of endogenous *EFCAB7* observed by immunofluorescence staining in RPE1 cells. The red fluorescence represents *EFCAB7*, while the green fluorescence represents Ac-tubulin (a marker of ciliary axoneme) and gamma-tubulin (a marker of the basal body). Scale bar: 20 μm and 2 μm. G, ciliary localization of EGFP-tagged *EFCAB7* or its mutant observed by immunofluorescence staining in RPE1 cells. Green represents *EFCAB7*, while red represents Ac-tubulin. Scale bar: 20 μm and 2 μm. H, effect of proteasome inhibitor MG132 (20 μM) on the level of *EFCAB7* and its mutant in transfected RPE1 cells. Quantification data presented below are based on three independent experimental repetitions. \*\*\**p* < 0.001, ns *p* > 0.05. I) Western blot analysis and quantification of the turnover rates of *EFCAB7* and its mutant in transfected RPE1 cells. Quantification data presented below are based on three independent experimental repetitions. \*\*\**p* < 0.001, ns *p* > 0.05.

# EFCAB7 splicing variant disrupts cilia function in heart development

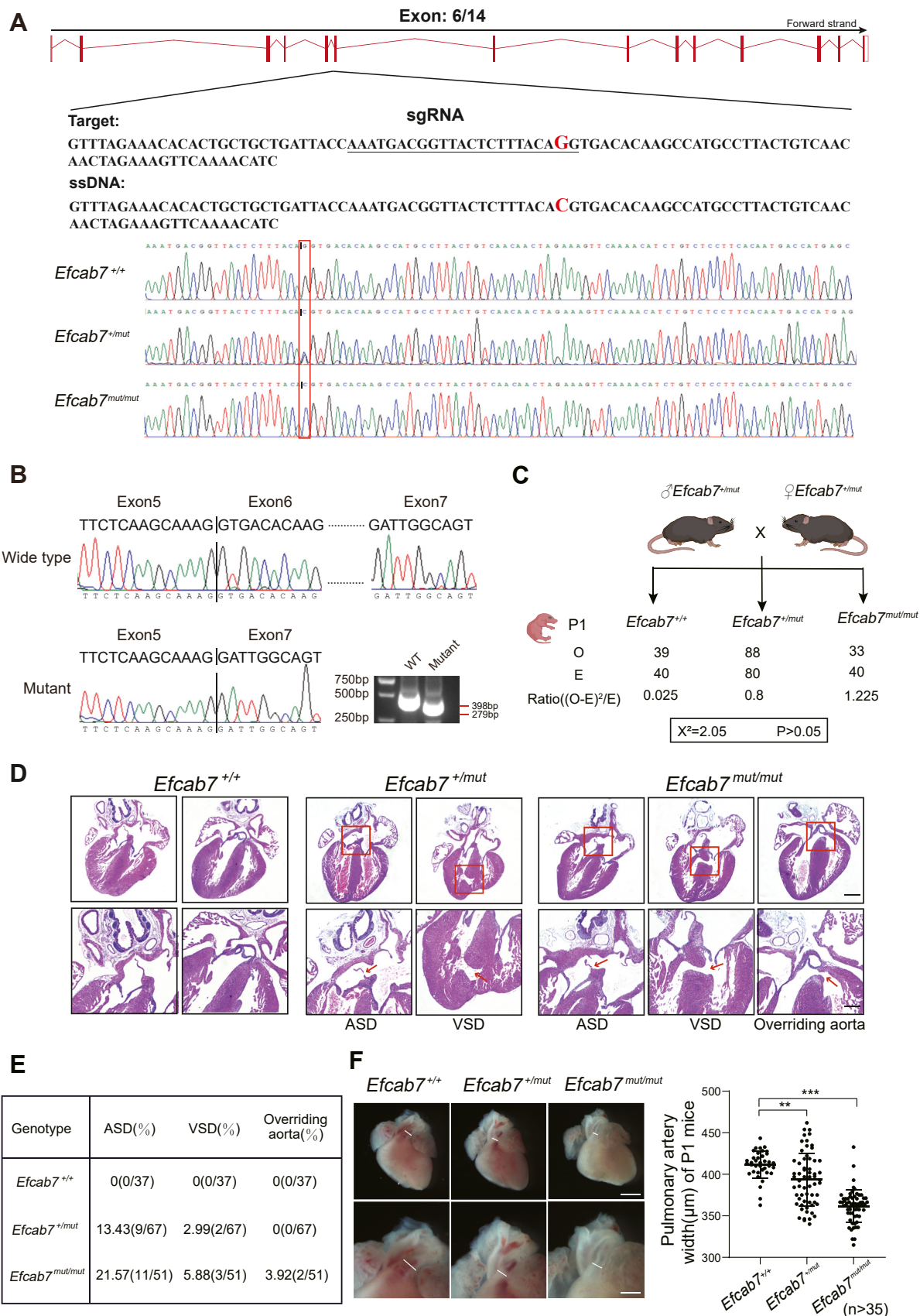


**Figure 2. Phenotypic analysis of *Efcab7* mutant mice.** A, validation of CRISPR/Cas9-mediated knock-in of the site variant at *Efcab7* locus. The schematic represents the target site and ssDNA sequence used for editing *Efcab7*. The lower panel shows the Sanger sequence analysis of gene-edited mice. B, verification of RT-PCR products from hearts of WT and *Efcab7* mutant mice by Sanger sequencing. An agarose gel electrophoresis image of RT-PCR products is presented. C, birth rate analysis of gene-edited *Efcab7* mice. O, the observed number of embryos; E, the expected number of embryos; Ratio= (O-E)<sup>2</sup>/E.

# EFCAB7 splicing variant disrupts cilia function in heart development

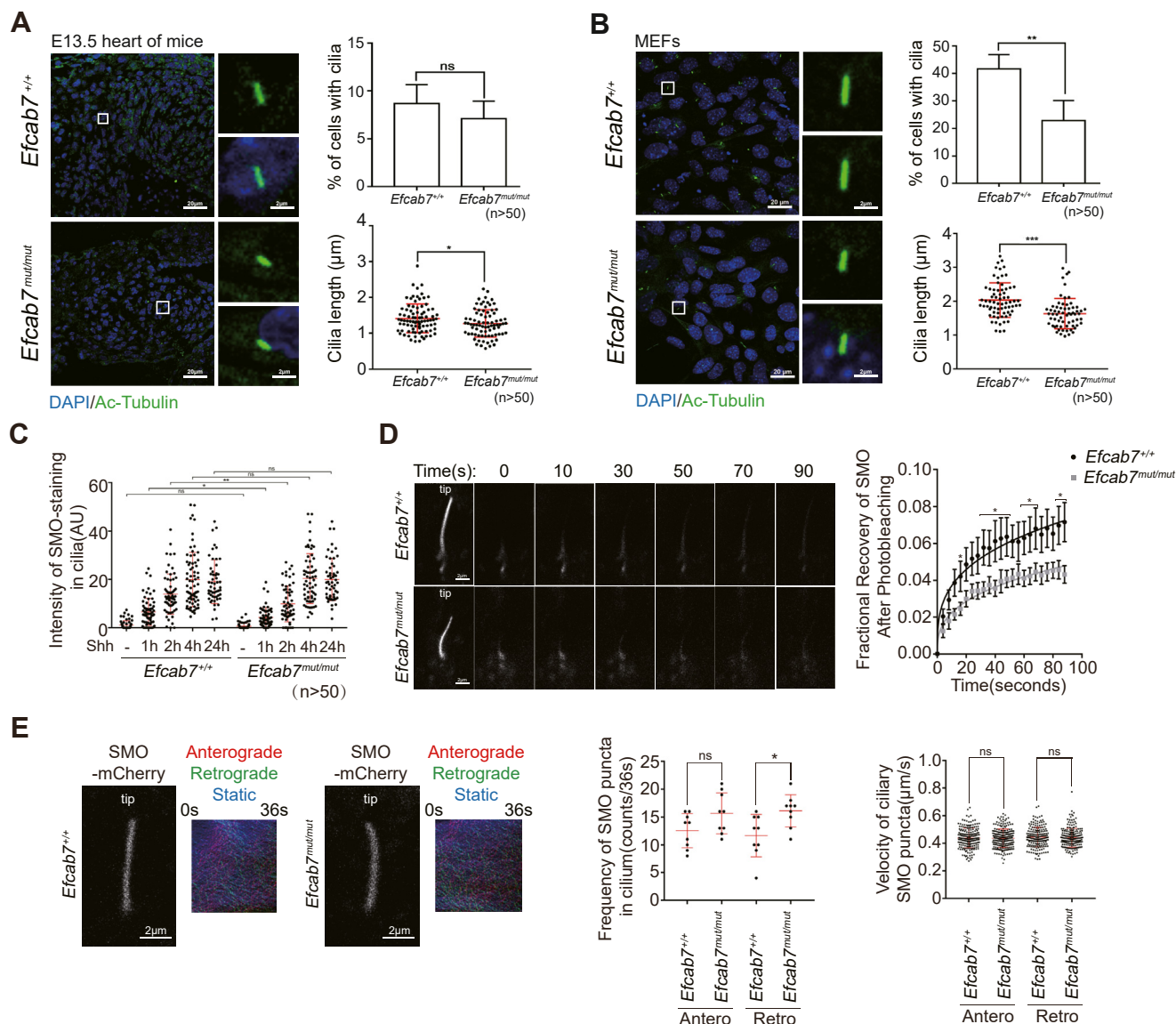


**Figure 3. Aberrant ciliogenesis in *Efcab7* mutant mice and cells.** A, representative immunofluorescent staining for primary cilia in the heart of WT and *Efcab7* mutant embryos at E13.5. Immunofluorescent staining of primary cilia in the E13.5 heart of WT and *Efcab7* mutant embryos. Quantification of percentage and ciliary length of ciliated cells from immunofluorescent staining. Scale bar: 20μm and 2μm. \**p* < 0.05, ns *p* > 0.05. B, representative immunofluorescent staining for primary cilia in primary MEFs isolated from E13.5 WT and *Efcab7* mutant embryos. Quantification of percentage and ciliary length of ciliated cells from immunofluorescent staining. Scale bar: 20μm and 2μm. \**p* < 0.05, \*\*\**p* < 0.001, ns *p* > 0.05. C, impaired ciliary transport of SMO in *Efcab7*<sup>mut/mut</sup> cells. Quantification of anti-SMO staining in primary cilia in WT and *Efcab7* mutant MEFs treated with Shh conditional medium for the indicated durations. (n > 50 in each group). Representative images shown in Fig. S3. \**p* < 0.05, \*\**p* < 0.01, ns *p* > 0.05. D, FRAP measurement of SMO-mCherry import into the primary cilium in WT and *Efcab7* mutant MEFs. The cells were treated with ShhN, and images of fluorescence recovery were captured every 2 s after photobleaching the entire cilium axoneme. Scale bar: 2μm. \**p* < 0.05. E, kymograms depicting the movement of SMO-mCherry particles in WT and *Efcab7* mutant MEFs. Scale bar: 2μm. \**p* < 0.05, ns *p* > 0.05.

products of *Myh6* (29), *Zfp1* (30) and *Nkx2-5* (8) in the E10.5 hearts of *Efcab7*<sup>mut/mut</sup> mice compared to WT mice (Fig. 4H).

The spatial transcriptomics (31) and scRNA-seq analysis of E10.5 hearts revealed distinct spatial expression patterns and subcellular localization of the three significantly down-regulated genes. *Myh6* and *Nkx2-5* were predominantly

expressed in cardiomyocytes, whereas *Zfp1* exhibited widespread coverage and uniform distribution throughout all regions of the cardiac outflow tract (Fig. 4, I–K). By conducting CUT&Tag analysis on E10.5 hearts of WT mice, we have obtained additional evidence supporting the interaction between *Gli1/2* and three significantly down-regulated genes

*P* > 0.05, the Chi-square test. D, heart phenotypes of P1 mice observed by HE staining. Magnified images of regions of interest are shown in the lower panel. The red arrow indicates the heart defect. E, statistical analysis of the cardiac phenotypes in WT, *Efcab7*<sup>+/mut</sup> and *Efcab7*<sup>mut/mut</sup> mice by exact probability method, *p* < 0.05. Scale bar: 500μm and 250μm. F, representative images of P1 hearts of gene-edited *Efcab7* mice under a stereoscope. The white lines indicate the measured sites of pulmonary artery width. Measurement of pulmonary artery width is presented. More than 35 P1 hearts from each group were selected for statistical analysis. Scale bar: 500μm and 1mm. \*\**p* < 0.01, \*\*\**p* < 0.001.



# EFCAB7 splicing variant disrupts cilia function in heart development

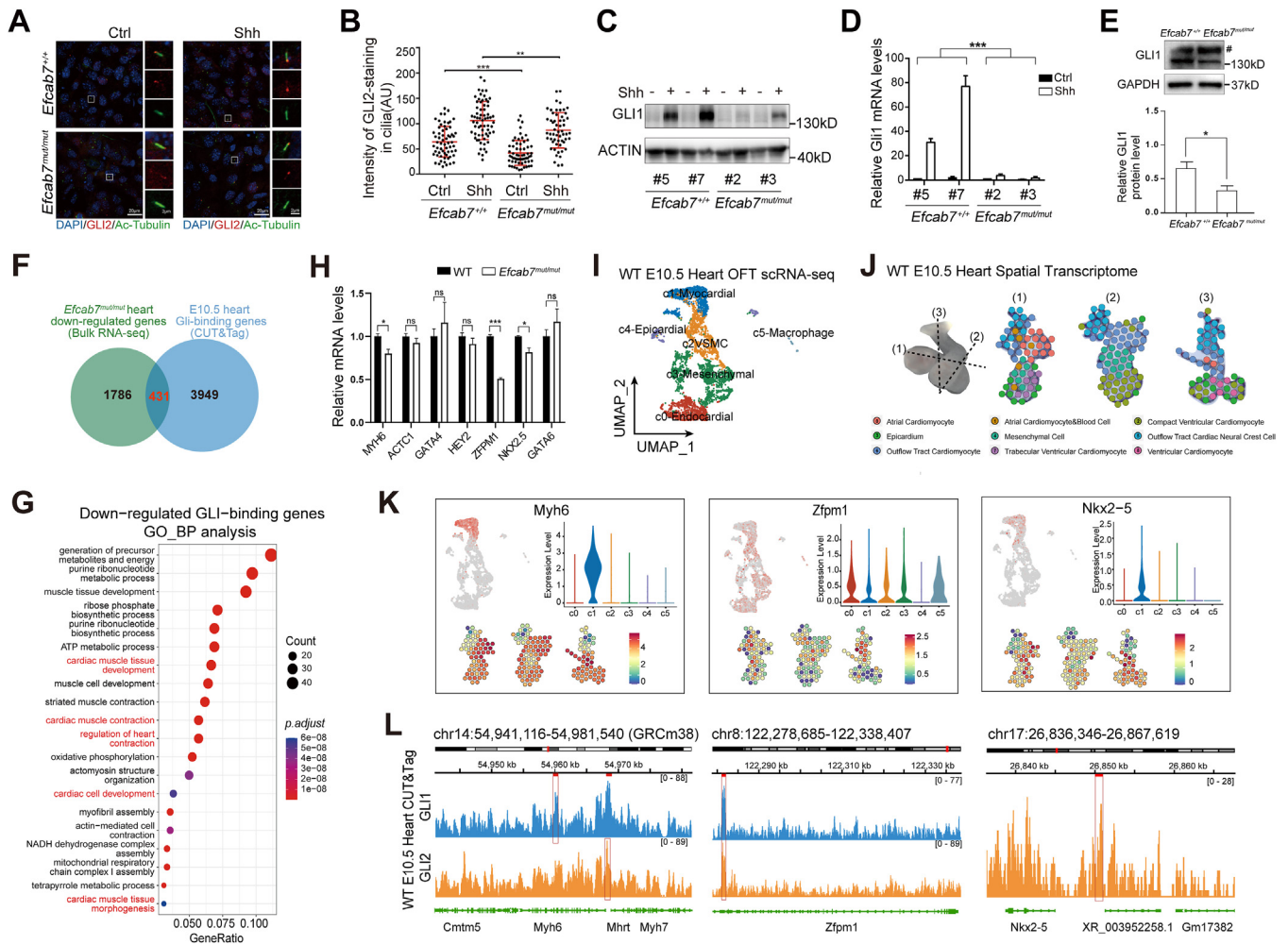


**Figure 4. *Efcab7* variant suppresses activation of Hh signaling in MEFs and embryonic hearts.** A, representative images of endogenous GLI2 immunostaining (red) in primary cilia (green, stained by anti-Ac-tubulin) in WT and *Efcab7* mutant MEFs in the absence or presence of ShhN. Scale bar: 20μm and 2μm. B, quantification of anti-GLI2 staining at the tip of primary cilia as shown in (A) (n > 50 per group). \*\*p < 0.01, \*\*\*p < 0.001. Western blot (C) and qPCR (D) analysis of *Gli1* expression in primary MEF cells induced by Shh. Primary MEF cells were isolated from embryos #5 and #7 of E13.5 *Efcab7*<sup>+/+</sup> (WT) or embryos #2 and #3 of *Efcab7*<sup>mut/mut</sup> (mutant) strains. \*\*\*p < 0.001. E, Western blot analysis of GLI1 expression in E10.5 WT and *Efcab7* mutant hearts. \*p < 0.05. # non-specific bands. F, Venn Diagram depicting significantly down-regulated genes identified in E10.5 *Efcab7*<sup>mut/mut</sup> hearts by bulk RNA-seq analysis (p.adjust < 0.05, FC < 1) and Gli-binding genes (*Gli1* and *Gli2*) identified by CUT&Tag analysis in E10.5 WT hearts (FDR < 0.05). G, the top 20 pathways in GO-Biological Process enrichment analysis of down-regulated GLI-binding genes. Pathways associated with heart development are highlighted in red. H, the relative mRNA expression of seven down-regulated GLI-binding genes, which have been reported to be associated with TOF, is presented. \*p < 0.05, \*\*\*p < 0.001. I, dimensionality reduction and clustering of single cells from E10.5 cardiac outflow tract, colored by cell types. J, a 10x spatial transcriptome cell type distribution map of E10.5 WT hearts. K, gene expression of three known genes associated with TOF (*Myh6*, *Zfp1* and *Nkx2-5*) was illustrated using scRNA-seq UMAP plot, a violin plot across scRNA-seq clusters, and spatial transcriptomics, respectively. L, IGV maps of the regulatory regions of *Gli1* and *Gli2* on these three target genes (*Myh6*, *Zfp1* and *Nkx2-5*), obtained by *Gli1* and *Gli2* CUT&Tag analysis of E10.5 WT hearts.

(*Myh6*, *Zfp1*, and *Nkx2-5*): Gli1 and Gli2 were observed to bind at the promoter region of *Zfp1*; Gli2 was observed to bind at the promoter region of *Myh6*, while Gli1 binding site was detected at the intro region of *Myh6*; moreover, Gli2 binding was found at the intergenic region of *Nkx2-5* (Fig. 4L). These findings revealed that the variant in *EFCAB7* may disrupt embryonic heart development by influencing downstream target genes (*Myh6*, *Zfp1*, and *Nkx2-5*) mediated through the Shh/Gli pathway.

## Discussion

In this study, we identified a splice site variant in the *EFCAB7* gene, which is associated with the role of primary cilia

in signaling, among Chinese patients with non-syndromic TOF. To elucidate the potential impact of this variant on cardiovascular development, we generated knock-in mice carrying the mutation. Through our analysis of cardiac phenotypes and underlying mechanisms, we further substantiated the crucial role of primary cilia in the pathogenesis of cardiac defects.

Through forward genetic screening in mice, it was discovered that numerous defects in ciliary genes could contribute to the development of congenital heart diseases, indicating a central role of ciliary defects in the pathogenesis of this condition (32, 33). Studies have demonstrated that cilia can dynamically interact with PCP components to regulate cell skeleton, thereby modulating cell polarity and the migration of

## EFCAB7 splicing variant disrupts cilia function in heart development

polarized cells (34). These dynamic cellular processes may facilitate the guidance of multiple extracardiac cell populations across significant distances toward the embryonic heart, which is crucial for normal heart development (13, 35). Primary cilia serve as chemosensory and mechanosensory organelles that coordinate multiple signaling pathways including HH, Wnt/PCP, Notch, and TGF- $\beta$ . They transmit signals between cells through various mechanisms such as cell membrane receptors, ion channels, and diverse G-protein-coupled receptors (19). Currently, the Shh signaling pathway represents one of the most well-described ciliary signaling pathways (36). Numerous studies have indicated that ablation or dysfunction of primary cilia can significantly impair Shh signaling. Mice lacking Shh exhibit phenotypes highly resembling TOF, characterized by ASD, VSD, and outflow tract defects along with abnormal aorta. Additionally observed are varying degrees of myocardial hypertrophy and abnormalities like pulmonary atresia or hypoplastic pulmonary artery (37, 38).

The Hedgehog pathway is closely associated with primary cilia and plays a crucial role in the development and separation of the cardiac outflow tract. The EFCAB7 protein has been demonstrated to interact with the EVC-EVC2 protein complex, facilitating its localization just distal to the ciliary transition zone and playing a pivotal role in the intra-ciliary transport of components of the Shh pathway (24). Mutations in *EFCAB7* lead to a reduction in both the number and length of cilia, thereby interfering with cilium-mediated expression of the Hedgehog pathway. In *Efcab7* knockout cells, Shh signal transduction is significantly inhibited, resulting in inaccurate localization of EVC-EVC2 ciliary proteins within the ciliary EVC zone as they become dispersed throughout the entire cilium (24). Our study confirms that loss-of-function variants

in human populations fail to sustain proper ciliary Shh signaling transduction. Although the variant does not significantly affect SMO's movement ability within cilia, it may impede SMO's import into cilia, leading to reduced accumulation on the ciliary membrane. This reduction markedly inhibits downstream activation of Gli transcription factors in the Shh pathway, consequently impairing normal heart development (Fig. 5). However, further investigation is required to determine whether this variant triggers abnormalities in other heart development-specific mechanisms.

In this study, we investigated the role of the *EFCAB7* gene in non-syndromic Tetralogy of Fallot (TOF). Through targeted genomic DNA sequencing, we identified variants of the *EFCAB7* gene in a cohort of TOF patients. Using a mini-gene vector and ectopic expression in cultured cell lines, we tested the molecular effects of the splicing variant on mRNA splicing and the resulting mutant protein on cilia morphology/Hh signaling. Additionally, the functional impact of this genetic variation on cardiac development was evaluated in mice carrying knock-in alleles. Along with cardiac morphology, we analyzed ciliogenesis, Hh signaling, and downstream gene expression in the mutant mice. Both *in vitro* and *in vivo* results confirm that *EFCAB7* is a novel candidate gene for TOF, with its disruption of cilia formation and downstream gene regulation playing a key role in disease pathology. This study represents the first report of a splicing variant in *EFCAB7* as a genetic cause of TOF, offering new insights into the functional mechanisms of ciliary genes in cardiac development and highlighting the potential for this variant to be used in future screening for congenital heart diseases.

Our study also has several limitations. First, during gene screening, we did not account for the possibility that a single

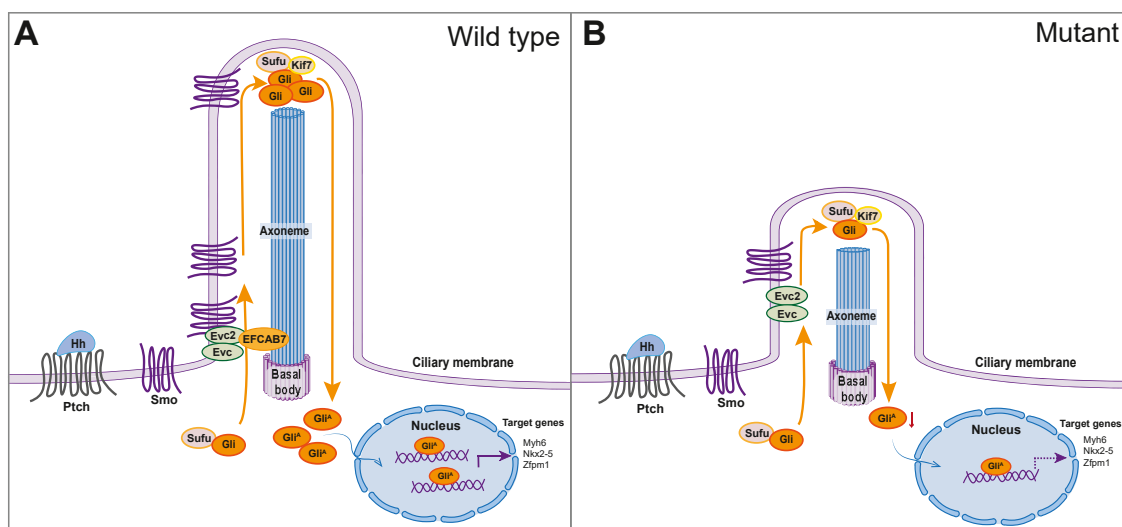


**Figure 5. Abnormal Hedgehog (Hh) signal transduction caused by *EFCAB7* mutation.** A, mechanism of Hedgehog Signaling Activity. Hedgehog signaling activity is primarily directed through the activated membrane protein receptor SMO, which, upon activation, stimulates the nuclear transcription factor Gli gene family. These Gli proteins then enter the nucleus and initiate the expression of downstream target genes. Notably, both the SMO receptor and Gli transcription factors are localized on the ciliary membrane or within the cilia. B, effect of *EFCAB7* Mutation on Hh Signaling. Mutation in *EFCAB7* leads to a decrease in the number and length of cilia, which subsequently impairs the cilia-mediated Hedgehog signaling pathway. The absence of EFCAB7 protein may hinder the transport of SMO within primary cilia, resulting in a significant reduction in the expression of the Gli transcription factor. Consequently, the decreased expression of Gli-binding target genes, such as *Myh6*, *Zfp1*, and *Nkx2-5*, leads to outflow tract dysplasia and congenital heart defects, including TOF.



patient might harbor multiple gene mutations. However, complex congenital heart diseases, including TOF, may be influenced by multiple gene mutations or gene-environment interactions. In this study, we focused solely on the mutation status of *EFCAB7* in our TOF population. Secondly, although we observed a certain proportion of cardiac defects in heterozygous mice, the incomplete penetrance observed in the patient population with TOF and mouse model prompted us to prioritize homozygous mice for subsequent mechanistic studies. We believe that homozygous mice offer advantages over heterozygous mice in exploring the potential downstream mechanisms of ciliary gene mutations that affect the pathogenesis of TOF. Therefore, all subsequent studies focus on homozygous mutant mice to investigate these downstream mechanisms. Future research could aim to address these limitations by considering the potential impact of multiple gene mutations and exploring the role of gene-environment interactions in the development of TOF.

In conclusion, our findings provide compelling evidence to support the pivotal involvement of *EFCAB7* in cardiac development through its regulation of ciliogenesis and Shh signaling transduction *via* primary cilia. These results suggest that *EFCAB7* holds promise as a potential candidate gene associated with congenital heart defects. Moreover, this study reinforces the crucial role played by primary cilia in orchestrating the complex process of cardiac septation during embryonic heart development.

## Experimental procedures

### Study patients

The study involved 131 TOF cases from Nanjing Children's Hospital and Jiangsu Provincial People's Hospital, and the other 682 patients with CHD were from the Second Affiliated Hospital of Nanjing Medical University. All cases were diagnosed by echocardiography or surgery. Cases with known chromosomal abnormalities, positive first-degree relatives with a family history of congenital heart defects, mothers exposed to pesticides or using therapeutic drugs during pregnancy, and mothers with diabetes or phenylketonuria were excluded. Individuals without heart diseases and other birth defects comprised the control group in the same area during the same period. Methods and experimental protocols involving human subjects were approved by the institutional review boards of Nanjing Medical University. All participants completed written informed consent form before taking part in this research, and all investigations conformed to the principles outlined in the Helsinki Declaration.

### DNA extraction and Sanger sequencing

Approximately 5 ml of peripheral blood was drawn from the subjects to extract genomic DNA, and the integrity of the DNA was detected by gel electrophoresis. We downloaded the coding region sequence of *EFCAB7* from the human reference genome (GRCh37/hg19) and used the online software Primer 3 (v.0.4.0) to design primers. The *EFCAB7*

coding region was amplified by PCR using 14 pairs of primers (Table S1). After the PCR reaction, the product was directly subjected to Sanger sequencing (Thingke, Nanjing). The sequencing data were visualized by the sequencing analysis (Application Biosystems), and the variants were analyzed using the online software NCBI Basic Local Alignment Search Tool (BLAST). The primer sequences for Sanger sequencing are listed in Table S1.

### Cells and plasmids

Primary mouse embryo fibroblasts (MEFs) were isolated from E13.5 mouse embryos of indicated genotypes. Human retinal pigment epithelial cells (RPE1) were presented by Xiumin Yan, Center of Excellence for Molecular Cells, Chinese Academy of Sciences. Human embryonic kidney cell 293T (HEK293T) is stored in our laboratory. *pRK5*, *pRK5-Shh*, *pEGFP-C2-EFCAB7*, and the mutant plasmids were constructed in our laboratory using homologous recombination technology.

### Generation of *Efcab7*<sup>mut/mut</sup> mice model using CRISPR-Cas9

All animal experiments were performed under the Guidelines for the Care and Use of Laboratory Animals and were approved by the Institutional Animal Care and Ethical Committee of Nanjing Medical University (IACUC-1912049). Anthropomorphic *Efcab7*<sup>mut/mut</sup> mice were generated by the CRISPR/Cas9 genome editing system. The sequences of *Efcab7* single-guide RNA (sgRNA: aaatgacggttactctttac) were designed by CRISPR Design (<http://crispr.mit.edu/>), and single-stranded oligodeoxynucleotide HDR template (ssDNA: gtttagaacaacactgctgctgattacaaatgacggttactctttacacgtgacacaagccatgccttactgtcaacaactagaagttcaaacatc) corresponding to this sequence was cloned into PGL3 for guide RNA *in-vitro* transcription. The edited sites were amplified by PCR and Sanger sequencing in the founders, and the founders were followed by at least three consecutive backcrosses with congenic mice (C57BL/6) to obtain a pure background. The conditional mutant allele was genotyped using forward primer: 5'-CCATTAAAGCCTGGTCAGTATGA-3' and reverse primer: 5'-GTTCAAACTCCATTGGTTCCC-3'. The animal study was reviewed and approved by the Institutional Animal Care and Use Committee of Nanjing Medical University.

### Histological analysis of mouse hearts

P1 hearts from WT and *Efcab7*<sup>mut/mut</sup> mice were isolated and fixed using 4% paraformaldehyde (PFA), dehydrated in a gradient of alcohol concentrations, embedded in paraffin using a paraffin embedding instrument (Thermo EC350), and sectioned frontally into 6-μm thick sections using a microtome (Thermo HM340E). Then, Hematoxylin and Eosin (H&E) staining was performed using an automatic dyeing device (Tissue-Tek DRS2000). The stained sections were sealed with neutral gum and photographed using a Zeiss microscope.

## EFCAB7 splicing variant disrupts cilia function in heart development

### Minigene splicing assay

According to the experimental procedure of MoBiTec GmbH in Germany, we amplified the genomic DNA (gDNA) fragment by PCR, which included exon5, exon6, and the intron located between them, and cloned them into an Exontrap Cloning Vector, pET01, for the minigene assay. The sequences of wild-type and mutant *EFCAB7* minigenes were validated using Sanger sequencing. The wild-type and mutant transcripts were produced by transient transfection of HEK293T cells with each plasmid. Total RNA was extracted from cells 48 hours after transfection and reverse-transcribed. Aberrantly spliced transcripts were identified by sequencing their RT-PCR products that were isolated *via* agarose gel electrophoresis.

### RNA extraction, reverse transcription, and quantitative PCR assay

Total RNA was isolated from cultured cells using the RNAiso reagent (TaKaRa). Reverse transcription was carried out using the Prime Script RT reagent Kit (TaKaRa). qPCR was performed using the FastStart SYBR Green Master Mix (Roche) on a LightCycler 96 System (Roche). The primers used to detect mRNA expression are listed in Table S5. Experiments were repeated at least three times, and samples were analyzed in triplicate.

### Immunofluorescence staining

Approximately  $0.6 \times 10^5$  cells per well were seeded onto Lab-Tek chambered slides and cultured for 24 h. The cells were transfected, allowed to recover for an additional 24 h, and then treated with ShhN-CM or other compounds, as indicated. Prior to any further treatments, the transfected cells were starved in pure DMEM for 24 h to visualize ciliary proteins. Following this, the cells were collected, and fixed in 4% PFA for 15 min at 4 °C, and processed using standard immunostaining procedures. The primary antibodies were: mouse anti-Acetylated tubulin (Sigma, 1:1000 dilution), mouse anti- $\gamma$ -tubulin (Sigma, 1:200 dilution), rabbit anti-EFCAB7 (Thermo Fisher Scientific, 1:100 dilution), mouse anti-Smo (Santa Cruz Biotechnology, 1:100 dilution), and goat anti-Gli2 (R&D Systems, 1:100 dilution). The secondary antibodies were as follows: anti-mouse IgG HRP (Santa Cruz Biotechnology, 1:200 dilution), anti-rabbit IgG HRP (Santa Cruz Biotechnology, 1:200 dilution), and anti-goat IgG HRP (Santa Cruz Biotechnology, 1:200 dilution).

### Live-cell imaging and fluorescence recovery after photobleaching

MEFs cultured for less than six passages were seeded onto 35-mm glass-bottom dishes. To imaging ciliary motility of SMO-mCherry, cells were infected with lentivirus for 48 h and then treated with a 1:9 mixture of Shh-containing medium and fresh medium for an additional 24 h to activate Shh signaling.

For live-cell imaging, ciliary images were captured at 300-ms intervals for 36 s using a ZEISS 900 microscope. Kymographs were generated from the time-lapse image sequence using

KymographClear 2.0 of Image J (Fiji). Particle velocities were measured from kymographs as the mean velocity. Traffic frequencies were determined from kymographs as the number of particles crossing the ciliary middle line per 36 s.

For Fluorescence Recovery After Photobleaching (FRAP) assay, ciliary m-Cherry was photobleached with a 594 nm laser, and cilia were observed using a ZEISS 900 microscope. Images were acquired every 2 s after photobleaching. Excluding the time for photobleaching, the total duration for the FRAP assay was 90 s. The signal intensities from cilia, cilia-photobleached regions, and background were measured using ImageJ (NIH).

### Protein extraction and Western blot analysis

After transfection or treatment as described above, cells were lysed in radioimmunoprecipitation assay buffer (RIPA buffer). Heart tissues from E10.5 mice were collected and lysed using the mammalian protein extraction reagent RIPA (Beyotime). Following centrifugation of the protein lysate, the protein in the supernatant was quantified using the BCA protein assay kit (Beyotime). Then, the lysates were denatured at 100 °C for 10 min with 6 × SDS loading buffer, subjected to SDS-PAGE, and subsequently analyzed by western blotting with the indicated antibodies, including rabbit anti-Gli1 (Cell Signaling Technology, 1:1000 dilution), rabbit anti- $\beta$ -actin (Affinity Biosciences, 1:1000 dilution), rabbit anti-GFP (Abcam, 1:1000 dilution), anti-mouse IgG HRP (Santa Cruz Biotechnology, 1:5000 dilution), and anti-rabbit IgG HRP (Santa Cruz Biotechnology, 1:5000 dilution).

### RNA-seq experiments and analysis

Total RNA was extracted using TRIzol (Thermo) treatment, and 2  $\mu$ g of total RNA per sample was used as input material for RNA sample preparations. The sequencing libraries were generated using the VAHTS mRNA-seq v2 Library Prep Kit (Illumina). The mRNA was purified from total RNA using poly-T oligo-magnetic beads and then cut into small fragments for cDNA synthesis. After adenylation of the 3' ends of the DNA fragments, adaptors with a hairpin loop structure were ligated and subjected to PCR amplification. High-throughput RNA sequencing was performed by using the Illumina Nova-Seq platform.

The raw data were filtered by Q30 quality score and aligned to the mouse reference genome GRCm38/mm10 using STAR software (v2.5.3a). Assembly and quantification of transcripts were performed using the RESM software (Version1.3.3) and were guided by the Ensembl GTF gene annotation file (<http://www.ensembl.org/>). The relative abundance of transcripts was measured using the number of fragments per million mapped reads (Fragments Per Kilobase of transcript per Million mapped reads, FPKM). Effectively expressed genes require an FPKM score greater than one.

### CUT&Tag experiment and high throughput sequencing

CUT&Tag experiment and high throughput sequencing were conducted by Seqhealth Technology Co., Ltd (Wuhan,

China). Two groups of samples, each containing 10 fresh E10.5 hearts from wild-type mouse embryos, were homogenized after collection to obtain cells, followed by incubation with Concanavalin A-coated magnetic beads. Next, cells were incubated with anti-GLI1 and anti-GLI2 primary antibody (GLI: R&D Systems, AF3324; GLI2: R&D Systems, AF3526) for 2 h, and then for 1 h with secondary antibody at room temperature. Hyperactive pG-Tn5 transposonase was then added to perform tagmentation. The reaction was terminated, and DNA fragments were extracted by PCI, followed by PCR amplification using indexed P5 and P7 primers. The library products were enriched, quantified, and finally sequenced on a Novaseq 6000 sequencer (Illumina) with PE150 mode.

Raw data were first filtered by Fastp (v0.23.1), discarding low-quality reads and trimming reads contaminated with adaptor sequences. Clean reads were mapped to the mouse reference genome GRCm38/mm10 using Bowtie2 (v2.2.6) with default parameters. Sambamba (v0.7.1) was then used for sam/bam format conversion and removal of PCR duplicate reads. DeepTools (v2.4.1) was employed to visualize the distribution of reads on upstream and downstream of TSS. The MACS2 software (v2.2.7.1) was used for peak calling, and bedtools (v2.30.0) for peak annotation and peak distribution analysis. The Homer (v4.10) was used for motifs analysis. Finally, by combining the motifs in JASPAR, the transcription factor binding sites were predicted by calling out the peak sequences of the potential target genes.

### Single-cell RNA sequencing (scrRNA-seq) analysis

Cardiac OFTs from E10.5 wild-type mouse embryos were dissected and transferred to a 2 ml Eppendorf tube containing tissue storage buffer (Miltenyi Biotec, #130–100–008). The tube was centrifuged at 50 g for 1 min at 4 °C. After discarding the tissue storage buffer, 1ml preheated digestion solution (Miltenyi Biotec, #130–110–203) at 37 °C was added to the OFTs tissue. The tube was incubated in a 37 °C water bath and gently pipetted three times every 5 min. The enzymatic incubation lasted for approximately 15 min. Upon completion, 10% FBS (Pricella, #164210–50) was added, and the solution was filtered using a 40-µm cell strainer (Corning, #CLS431750). The suspensions were centrifuged at 300g for 3 min at 4 °C, and the pellets were resuspended in PBS with 0.01% Bovine serum albumin (Sigma, #A1933).

Then cells were loaded into microfluidic chip of Chip A Single Cell Kit v2.0 (MobiDrop, #S050100201) to generate droplets with MobiNova-100 (MobiDrop, #A1A40001). Each cell was encapsulated into a droplet which contained a gel bead linked with up to millions of oligos (cell unique barcode). After encapsulation, the droplets were exposed to light from the MobiNovaSP-100 (MobiDrop, #A2A40001) for cutting while oligos diffused into the reaction mix. The mRNAs were captured *via* cell barcodes, with cDNA amplification occurring within the droplets. Following reverse transcription, cDNAs with barcodes were amplified, and a library was constructed using the High Throughput Single Cell 3'RNA-Seq Kit v2.0 (MobiDrop, #S050200201) and the 3' Single Index Kit

(MobiDrop, #S050300201). The resulting libraries were sequenced on an Illumina NovaSeq 6000 System.

The raw FASTQ files were de-multiplexed and mapped to the mouse reference genome GRCm38/mm10 by Cell Ranger (v.6.1.1) pipeline with default parameters to generate the feature-barcode gene expression matrix. Cell filtering, data normalization, and unsupervised analysis were carried out in R package Seurat (v4.1.3) according to their recommended steps. In brief, genes expressed in less than 3 cells, and cells with <200 genes or >10% mitochondrial genes were filtered out. Doublets were detected and removed using R package DoubletFinder (v2.0.3). The Harmony R package (v0.1.1) was used for batch correction to avoid the batch effect of sample identity, which might disrupt the downstream analysis. A subset of 11 significant principal components was selected using the Seurat ElbowPlot and JackStrawPlot functions. Cell clustering and UMAP visualization were performed using Seurat FindClusters and RunUMAP functions. To identify specific genes for each cell cluster, we applied the Seurat FindAllMarkers function using the default parameters. The annotations of cell identity on each cluster were defined by the expression of known marker genes.

### Statistical analysis

Statistical analyses were performed with GraphPad Prism 7.0. Each measurement was repeated at least three times. Comparisons between indicated groups were performed using the Wilcoxon-Mann-Whitney test. *p* values < 0.05 were considered statistically significant. \**p* < 0.05, \*\**p* < 0.01, \*\*\**p* < 0.001 and ns for *p* > 0.05.

### Data availability

All data generated or analyzed during this study are included in this published article and its additional files.

**Supporting information**—This article contains supporting information.

**Acknowledgments**—We would like to thank Bin Shen from the State Key Laboratory of Reproductive Medicine of Nanjing Medical University for the Exontrap system, and Xiumin Yan from the Center of Excellence for Molecular Cells, Chinese Academy of Sciences for the RPE1 cell line.

**Author contributions**—Z. H., S. Y., B. Z., and Y. G. conceptualization; Z. H., S. Y., B. Z., and Y. G. methodology; X. Y., Q. W., and T. L. validation; X. Y., Q. W., T. L., Y. Z., and J. G. formal analysis; X. Y., Q. W., T. L., W. M., N. Z., X. L., Z. A., and S. Y. C. investigation; X. Y., Q. W., and T. L. writing—original draft; X. Y., Q. W., T. L., Y. Z., and J. G. visualization; Y. Z. and J. G. data curation; Z. H., S. Y., and Y. G. writing—review & editing.

**Funding and additional information**—This work was supported by Program of the National Key Project of Research and Development Program (2021YFC2700600); the Science Fund Program for Distinguished Young Scholars of the National Natural Science Foundation of China (82322032); the National Natural Science Foundation of China (82471890, 82173291, 82172629, and



# EFCAB7 splicing variant disrupts cilia function in heart development

82373420); the Natural Science Foundation of Shandong Province (ZR2020KH032); and Jiangsu Commission of Health (Z2020035).

**Conflict of interest**—The authors declare that they have no conflicts of interest with the contents of this article.

**Abbreviations**—The abbreviations used are: ASD, atrial septal defect; CHD, congenital heart defects; CHX, cycloheximide; EFCAB7, EF-hand calcium binding domain 7; EvC, Ellis van Creveld; FRAP, fluorescence Recovery After Photobleaching; gDNA, genomic DNA; HEK293T, human embryonic kidney cell 293T; Hh, Hedgehog; MEFs, mouse embryo fibroblasts; OFT, outflow tract; P1, postnatal day 1; PFA, paraformaldehyde; RPE1, human retinal pigment epithelial cells; sgRNA, single-guide RNA; Shh, Sonic Hedgehog; TOF, Tetralogy of Fallot; VSD, ventricular septal defect; WB, western blot; WT, wild-type.

## References

- Mitchell, S. C., Korones, S. B., and Berendes, H. W. (1971) Congenital heart disease in 56,109 births. Incidence and natural history. *Circulation* **43**, 323–332
- van der Linde, D., Konings, E. E., Slager, M. A., Witsenburg, M., Helbing, W. A., Takkenberg, J. J., *et al.* (2011) Birth prevalence of congenital heart disease worldwide: a systematic review and meta-analysis. *J. Am. Coll. Cardiol.* **58**, 2241–2247
- Collaborators, G. C. H. D. (2020) Global, regional, and national burden of congenital heart disease, 1990–2017: a systematic analysis for the Global Burden of Disease Study 2017. *Lancet Child Adolescent Health* **4**, 185–200
- Bruneau, B. G. (2008) The developmental genetics of congenital heart disease. *Nature* **451**, 943–948
- Apitz, C., Webb, G. D., and Redington, A. N. (2009) Tetralogy of Fallot. *Lancet (London, England)* **374**, 1462–1471
- Shabana, N. A., Shahid, S. U., and Irfan, U. (2020) Genetic contribution to congenital heart disease (CHD). *Pediatr. Cardiol.* **41**, 12–23
- Morgenthau, A., and Frishman, W. H. (2018) Genetic origins of tetralogy of Fallot. *Cardiol. Rev.* **26**, 86–92
- Page, D. J., Miossec, M. J., Williams, S. G., Monaghan, R. M., Fotiou, E., Cordell, H. J., *et al.* (2019) Whole exome sequencing reveals the major genetic contributors to nonsyndromic tetralogy of Fallot. *Circ. Res.* **124**, 553–563
- Vergara, P., Digilio, M. C., De Zorzi, A., Di Carlo, D., Capolino, R., Rimini, A., *et al.* (2006) Genetic heterogeneity and phenotypic anomalies in children with atrioventricular canal defect and tetralogy of Fallot. *Clin. Dysmorphol.* **15**, 65–70
- Mercer-Rosa, L., Paridon, S. M., Fogel, M. A., Rychik, J., Tanel, R. E., Zhao, H., *et al.* (2015) 22q11.2 deletion status and disease burden in children and adolescents with tetralogy of Fallot. *Circ. Cardiovasc. Genet.* **8**, 74–81
- Homsy, J., Zaidi, S., Shen, Y., Ware, J. S., Samocha, K. E., Karczewski, K. J., *et al.* (2015) De novo mutations in congenital heart disease with neurodevelopmental and other congenital anomalies. *Science (New York, N.Y.)* **350**, 1262–1266
- Tang, C. S. M., Mononen, M., Lam, W. Y., Jin, S. C., Zhuang, X., Garcia-Barcelo, M. M., *et al.* (2022) Sequencing of a Chinese tetralogy of Fallot cohort reveals clustering mutations in myogenic heart progenitors. *JCI insight* **7**, e152198
- Klena, N. T., Gibbs, B. C., and Lo, C. W. (2017) Cilia and ciliopathies in congenital heart disease. *Cold Spring Harb. Perspect. Biol.* **9**, a028266
- Slough, J., Cooney, L., and Brueckner, M. (2008) Monocilia in the embryonic mouse heart suggest a direct role for cilia in cardiac morphogenesis. *Dev. Dyn.* **237**, 2304–2314
- Del Viso, F., Huang, F., Myers, J., Chalfant, M., Zhang, Y., Reza, N., *et al.* (2016) Congenital heart disease genetics uncovers context-dependent organization and function of nucleoporins at cilia. *Dev. Cell* **38**, 478–492
- Singla, V., and Reiter, J. F. (2006) The primary cilium as the cell's antenna: signaling at a sensory organelle. *Science (New York, N.Y.)* **313**, 629–633
- Eggenchwil, J. T., and Anderson, K. V. (2007) Cilia and developmental signaling. *Annu. Rev. Cel. Dev. Biol.* **23**, 345–373
- Kopinke, D., Norris, A. M., and Mukhopadhyay, S. (2021) Developmental and regenerative paradigms of cilia regulated hedgehog signaling. *Semin. Cel. Dev. Biol.* **110**, 89–103
- Mill, P., Christensen, S. T., and Pedersen, L. B. (2023) Primary cilia as dynamic and diverse signalling hubs in development and disease. *Nat. Rev. Genet.* **24**, 421–441
- Rohatgi, R., Milenkovic, L., and Scott, M. P. (2007) Patched1 regulates hedgehog signaling at the primary cilium. *Science (New York, N.Y.)* **317**, 372–376
- Hildebrandt, F., Benzing, T., and Katsanis, N. (2011) Ciliopathies. *New Engl. J. Med.* **364**, 1533–1543
- Ferkol, T. W., and Leigh, M. W. (2012) Ciliopathies: the central role of cilia in a spectrum of pediatric disorders. *J. Pediatr.* **160**, 366–371
- Bilal, M., Khan, H., Khan, M. J., Haack, T. B., Buchert, R., Liaqat, K., *et al.* (2023) Variants in EFCAB7 underlie nonsyndromic postaxial polydactyly. *Eur. J. Hum. Genet.* **31**, 1270–1274
- Pusapati, G. V., Hughes, C. E., Dorn, K. V., Zhang, D., Sugianto, P., Aravind, L., *et al.* (2014) EFCAB7 and IQCE regulate hedgehog signaling by tethering the EVC-EVC2 complex to the base of primary cilia. *Dev. Cell* **28**, 483–496
- Nguyen, T. Q., Saitoh, M., Trinh, H. T., Doan, N. M., Mizuno, Y., Seki, M., *et al.* (2016) Truncation and microdeletion of EVC/EVC2 with missense mutation of EFCAB7 in Ellis-van Creveld syndrome. *Congenit. Anom.* **56**, 209–216
- Nguyen, T. Q. N., Doan, N. M. T., Trinh, H. T., and Mizuguchi, M. (2019) Novel mutation in EFCAB7 alters expression and interaction of Ellis-van Creveld ciliary proteins. *Congenit. Anom.* **59**, 49–50
- Goddeeris, M. M., Schwartz, R., Klingensmith, J., and Meyers, E. N. (2007) Independent requirements for Hedgehog signaling by both the anterior heart field and neural crest cells for outflow tract development. *Development (Cambridge, England)* **134**, 1593–1604
- Toomer, K. A., Fulmer, D., Guo, L., Drohan, A., Peterson, N., Swanson, P., *et al.* (2017) A role for primary cilia in aortic valve development and disease. *Dev. Dyn.* **246**, 625–634
- Chaithra, S., Agarwala, S., and Ramachandra, N. B. (2022) High-risk genes involved in common septal defects of congenital heart disease. *Gene* **840**, 146745
- Goldmuntz, E., Geiger, E., and Benson, D. W. (2001) NKX2.5 mutations in patients with tetralogy of Fallot. *Circulation* **104**, 2565–2568
- Gu, Y., Zhou, Y., Ju, S., Liu, X., Zhang, Z., Guo, J., *et al.* (2022) Multi-omics profiling visualizes dynamics of cardiac development and functions. *Cell Rep.* **41**, 111891
- Li, Y., Klena, N. T., Gabriel, G. C., Liu, X., Kim, A. J., Lemke, K., *et al.* (2015) Global genetic analysis in mice unveils central role for cilia in congenital heart disease. *Nature* **521**, 520–524
- Willaredt, M. A., Gorgas, K., Gardner, H. A., and Tucker, K. L. (2012) Multiple essential roles for primary cilia in heart development. *Cilia* **1**, 23
- Cui, C., Chatterjee, B., Lozito, T. P., Zhang, Z., Francis, R. J., Yagi, H., *et al.* (2013) Wdpcp, a PCP protein required for ciliogenesis, regulates directional cell migration and cell polarity by direct modulation of the actin cytoskeleton. *PLoS Biol.* **11**, e1001720
- Djenoune, L., Berg, K., Brueckner, M., and Yuan, S. (2022) A change of heart: new roles for cilia in cardiac development and disease. *Nat. Rev. Cardiol.* **19**, 211–227
- Bangs, F., and Anderson, K. V. (2017) Primary cilia and mammalian hedgehog signaling. *Cold Spring Harbor Perspect. Biol.* **9**, a028175
- Washington Smoak, I., Byrd, N. A., Abu-Issa, R., Goddeeris, M. M., Anderson, R., Morris, J., *et al.* (2005) Sonic hedgehog is required for cardiac outflow tract and neural crest cell development. *Developmental Biol.* **283**, 357–372
- Tsukui, T., Capdevila, J., Tamura, K., Ruiz-Lozano, P., Rodriguez-Esteban, C., Yonei-Tamura, S., *et al.* (1999) Multiple left-right asymmetry defects in Shh(-/-) mutant mice unveil a convergence of the shh and retinoic acid pathways in the control of Lefty-1. *Proc. Natl. Acad. Sci. U. S. A.* **96**, 11376–11381